Acta Crystallographica Section D
Biological Crystallography
ISSN 0907-4449

Measurable characteristics of lysozyme crystal growth

Sridhar Gorti,[a]* Elizabeth L. Forsythe[b] and Marc L. Pusey[a]

[a]National Aeronautics and Space Administration, Huntsville, AL 35812, USA, and [b]BAE SYSTEMS at MSFC, Physical and Biological Sciences Laboratory, NASA/MSFC, Huntsville, AL 35812, USA

Correspondence e-mail: sridhar.gorti-1@nasa.gov

Received 23 September 2004
Accepted 1 March 2005

The behavior of protein crystal growth is estimated from measurements performed at both the microscopic and molecular levels. In the absence of solutal flow, it was determined that a model that balances the macromolecular flux toward the crystal surface with the flux of the crystal surface well characterizes crystal growth observed using microscopic methods. Namely, it was determined that the model provides accurate estimates for the crystal-growth velocities upon evaluation of crystal-growth measurements obtained in time. Growth velocities thus determined as a function of solution supersaturation were further interpreted using established deterministic models. From analyses of crystal-growth velocities, it was found that the mode of crystal growth varies with respect to increasing solution supersaturation, possibly owing to kinetic roughening. To verify further the hypothesis of kinetic roughening, crystal growth at the molecular level was examined using atomic force microscopy (AFM). From the AFM measurements, it was found that the magnitude of surface-height fluctuations, $h(x)$, increases with increasing solution supersaturation. In contrast, the estimated characteristic length, ξ, decreases rapidly upon increasing solution supersaturation. It was conjectured that the magnitude of both $h(x)$ and ξ could possibly determine the mode of crystal growth. Although the data precede any exact theory, the non-critical divergence of $h(x)$ and ξ with respect to increasing solution supersaturation was nevertheless preliminarily established. Moreover, approximate models to account for behavior of both $h(x)$ and ξ are also presented.

1. Introduction

Analyses of lysozyme crystal-growth rates or velocities using standard models indicated the possibility of kinetic roughening in lysozyme-crystal growth (Gorti, Forsythe *et al.*, 2004, 2005; Gorti, Konnert *et al.*, 2005). Namely, it was determined that tetragonal lysozyme crystals grown above a crossover supersaturation σ_c (where supersaturation $\sigma = \ln c/c_{eq}$ and c and c_{eq} are the solution and solubility concentration, respectively; see Table 1 for definitions) exhibit microscopically rough surfaces due to the continuous addition of growth units anywhere on the surface of a crystal. The crystal-growth velocity, V_c, for a continuous growth process is determined by the continuous flux of macromolecules onto a unit area of the crystal surface, a^2, due to diffusion, D, and a probability of attachment, expressed as (Gorti *et al.*, 2004; Gorti, Forsythe *et al.*, 2005)

$$V_c(c, T) = \frac{N_A D a^2}{1.6 M_w \varphi^{-1/3}} [c - c_r(T)] \exp(-E_c/k_B T). \quad (1)$$

The definitions of variables are as follows: N_A is Avogadro's number, E_c is the energy barrier for attachment, $k_B T$ is thermal energy and a, M_w and φ are the radius, molecular weight and volume fraction of the macromolecule, respectively. The prefactor $[c - c_r(T)]$ is a limit imposed within the model that describes linear growth by continuous addition for solution conditions that exceed a crossover concentration $c_r(T)$ or supersaturation, σ_c, defined as $\sigma_c = \ln(c_r/c_{eq})$.

Below σ_c, however, a two-dimensional nucleation model was applied to accurately predict the measured crystal-growth rates. In the two-dimensional nucleation model, layer-by-layer growth of a planar crystal surface is dependent on step generation by the

Table 1
Summary of definitions.

a (cm)	Linear dimension or radius of molecule
c (mg ml^{-1}), c_∞	Prepared concentration of protein solution
c_{eq} (mg ml^{-1})	Solubility or equilibrium concentration
c_r (mg ml^{-1})	Kinetic crossover concentration
$C(x)$	Spatial correlation function
ΔG^*_{2Dnuc}	Two-dimensional nucleation free-energy barrier at maximum
$\Delta\mu$, σ	Disequilibrium $\Delta\mu = k_BT\sigma$ or excess supersaturation, $\sigma = \ln(c/c_{eq})$
D (cm^2 s^{-1})	Solute diffusion coefficient
E_c (erg/molecule)	Energy barrier determining the probability of macromolecular attachment in crystal growth in the continuous mode
E_s (erg/molecule-cm)	Energy barrier per unit length determining the probability of macromolecular attachment at a kink or step edge for crystal growth in the layer mode
γ (erg/molecule)	Effective energy barrier, $\gamma = E_s\Omega^{1/2}$
h, $h(x)$	Step height and height as a function of position, x
$(\langle h^2\rangle - \langle h\rangle^2)^{1/2}$	Root-mean-square (r.m.s.) magnitude of fluctuations
j_{in}, j_{crys}	Solutal flux towards the crystal and crystal flux into the solution, respectively
J	Nucleation rate or rate of formation of two-dimensional nucleates on the surface of a crystal
N^*_{2Dnuc}	Number of molecules in a critical two-dimensional nucleate
σ_c	The critical crossover supersaturation $\ln(c_r/c_{eq})$
T_{dev}	Temperature at deviation point in the growth velocity data
V_s (cm s^{-1})	Growth velocity or rate normal to the surface of a smooth crystal in growth by layers generated by two-dimensional nucleation
V_x, V_c (cm s^{-1})	Growth velocity normal to the surface and growth velocity normal to the surface of a rough crystal in growth by continuous mode, respectively
ξ	Spatial correlation length

formation of stable two-dimensional nucleates and incorporation of growth units at the step edge. The growth velocity normal to a planar surface, V_s, is expressed as (Saito, 1996)

$$V_s(c, T) = Ac_{eq}^{1/3}\exp\left(\frac{2\Delta\mu}{3k_BT}\right)\left(\frac{\Delta\mu}{k_BT}\right)^{1/6} \times\left[\exp\left(\frac{\Delta\mu}{k_BT}\right)-1\right]^{2/3}\exp\left(-\frac{\pi\gamma^2}{3\Delta\mu k_BT}\right). \quad (2)$$

The effective barrier for growth by two-dimensional nucleation $\gamma = E_s\Omega^{1/2}$, where Ω is the attachment unit area at a lattice site and E_s is the step-free energy per unit length and $\Delta\mu$ (= $k_BT\ln c/c_{eq}$) is the solution disequilibrium. The pre-factor A accounts for the frequency with which a macromolecule attempts to overcome a barrier for step generation and advancement and is related to surface diffusive processes.

On the basis of the models applied, the energetics of lysozyme crystal growth was determined for both the (110) and (101) faces of tetragonal lysozyme (Gorti *et al.*, 2004; Gorti, Forsythe *et al.*, 2005). From such determinations, we found that the magnitudes of the energy barrier for the continuous addition of molecules anywhere on the crystal surface, E_c, for both (110) and (101) faces were comparable, $E_c \simeq 6 \pm 1 \times 10^{-13}$ erg/molecule, whereas the magnitude of γ varied marginally for the two faces, $\gamma(110) = 1.3 \pm 0.3 \times 10^{-13}$ erg/molecule and $\gamma(101) = 1.0 \pm 0.2 \times 10^{-13}$ erg/molecule. The magnitude of σ_c, while essentially invariant with respect to the solution pH, temperature or precipitant concentration, also varied for the two faces, $\sigma_c(110) = 1.9 \pm 0.2$ and $\sigma_c(101) = 1.7 \pm 0.2$.

The experimentally determined magnitudes for the crossover supersaturation, σ_c, and the effective barrier for growth by two-dimensional nucleation, γ, are significant for the evaluation of concepts promoting kinetic roughening. For example, at temperatures below the equilibrium thermodynamic roughening temperature, T_r, kinetic roughening occurs as the magnitude of the Gibb's free energy for the formation of a two-dimensional nucleate at maximum, ΔG^*_{2Dnuc}, is less than or equal to the thermal energy, k_BT (Elwenspoek & van der Eerden, 1987; Bennema, 1993; Liu *et al.*, 1993; Liu & Bennema, 2001). When $\Delta G^*_{2Dnuc} \leq k_BT$, the 'size' of the two-dimensional nucleate is expected to be the 'size' of the adatom, N^*_{2Dnuc} (Levi & Kotrla, 1997; Tartaglino & Levi, 2000). Hence, upon attachment, every adatom formed on the surface is stable and will subsequently grow. The two-dimensional nucleation free-energy barrier at maximum, ΔG^*_{2Dnuc}, and the number of molecules in a critical two-dimensional nucleate, N^*_{2Dnuc}, are given by (Saito, 1996)

$$\Delta G^*_{2Dnuc} = \pi\gamma^2/\Delta\mu, \quad N^*_{2Dnuc} = \pi\gamma^2/\Delta\mu^2. \quad (3)$$

(3) is only applicable for temperatures below T_r, as both σ and γ_σ are zero at the thermodynamic roughening temperature, T_r (Bennema, 1993). For all $T \geq T_r$, crystal growth proceeds by continuous addition for $\sigma > 0$, as $\gamma = 0$ (Bennema, 1993). The significance of (3) is that at $T < T_r$, $\gamma > 0$ and the diminishing of $\Delta G^*_{2Dnuc} \leq k_BT$ occurs when $\Delta\mu = k_BT\sigma$ increases up to σ_c (Bennema, 1993). Using estimated values for γ and σ_c for all conditions investigated, $N^*_{2Dnuc} = 7 \pm 2$ at 295 K and $\Delta G^*_{2Dnuc} >> k_BT$ (Gorti *et al.*, 2004; Gorti, Forsythe *et al.*, 2005; Gorti, Konnert *et al.*, 2005). However, if the estimated values for γ and E_c were normalized with respect to N^*_{2Dnuc}, (3) yields $\Delta G^*_{2Dnuc} \simeq 1 \times 10^{-14}$ erg/molecule or $\sim 0.3k_BT$ at 295 K. Hence the hypothesis that the crossover to continuous mode growth occurs at the diminishment of $\Delta G^*_{2Dnuc} \leq k_BT$ is supported, but only upon normalization of γ with respect to N^*_{2Dnuc}.

While growth-velocity data as well as observations of rough or rounded surfaces are considered as compelling evidence in support of kinetic roughening, the data are by no means rigorously conclusive. Although the present concern does not detract from the overall finding of kinetic roughening, we nevertheless believe that a detailed evaluation of experimental measurements as well as alternative approaches for determining kinetic roughening is warranted. Hence, in this effort, we describe several measurable characteristics of crystal growth observed at both the microscopic and molecular level. As such, the manuscript is thus organized as follows: §2 presents a discussion of the possible errors in the microscopic measurements of crystal-growth velocities, §3 is a discussion of a method for the estimation of the magnitude of γ and E_c from microscopic measurements of crystal-growth velocities as well as the determination of c_r and §4 presents a preliminary application of atomic force microscopy in the possible determination of the energetics of crystal growth as well as kinetic roughening of crystal surfaces.

2. Measurement of crystal-growth rate or velocity

Several microscopic methods have been applied in the measurement of crystal-growth velocities (Durbin & Feher, 1986; Pusey *et al.*, 1986; Durbin & Carlson, 1992; Monaco & Rosenberger, 1993; Vekilov, 1993; Konnert *et al.*, 1994; Kurihara *et al.*, 1996; Kuznetsov *et al.*, 1996). Regardless of the method applied, the precision with which crystal-growth velocity measurements can be obtained is considered to be dependent on both the growth velocity as well as solution conditions. The measurement of crystal-growth velocities as well as inherent uncertainties in such measurements is thus discussed in this section. In particular, the effect of the formation of a 'depletion' zone on the accuracy of crystal-velocity determinations is considered. The assumption applied in the current discussion is that growth velocity measurements are performed in quiescent solutions in the absence of convection, a limiting case.

Consider, for example, the measurement of crystal-growth velocities using optical microscopy. Fig. 1 displays data obtained upon measurement of crystal growth in time for 0.1 *M* sodium acetate

(NaAc), 4%(*w*/*v*) sodium chloride (NaCl) at pH 5.0 for an excess protein concentration $c/c_{eq} \simeq 12$. Prior to data collection, buffered precipitant (NaCl) was added to a concentrated lysozyme solution, in 0.1 *M* NaAc pH 5.0, to yield a final concentration of 60 mg ml^{-1} lysozyme with 4%(*w*/*v*) NaCl. The freshly prepared solution was then filtered and injected into a sample holder containing pre-grown lysozyme seed crystals (~10–20 µm), replacing solution used for their preparation. At periodic intervals, digital images were taken and subsequently analyzed to determine the extent of crystal growth. As shown in Fig. 1, the linear dimension of the 110 face of lysozyme crystals increased linearly over ~30 min. The slope obtained from a linear fit to data determined the growth velocity (1.1×10^{-6} cm s^{-1}) of the (110) face.

Indeed, all reported measurements of crystal-growth velocities using optical microscopy were determined using a linear fit to the growth data (Forsythe & Pusey, 1994; Forsythe *et al.*, 1994; Nadarajah *et al.*, 1995; Forsythe, Nadarajah *et al.*, 1999), as illustrated in Fig. 1. Predominantly, crystal faces grow linearly over a given observation period. In few instances, however, nonlinearities in crystal growth over prolonged observation times were noted. Under such circumstances, the observation times were either truncated or limited to shorter times (order of minutes) to justify a linear fit to the growth data. The solution conditions that often gave rapid rise to a non-linear behavior in crystal growth were of high precipitant and low protein concentration that exhibited high near-maximal growth velocities. The non-linear behavior in crystal growth can be understood in qualitative terms for the limiting case where crystal growth in supersaturated solutions is governed by a mass balance between the rate of protein attachment and protein diffusion.

When the kinetics of protein attachment on the crystal surface are more rapid than the diffusivity of proteins towards the growing surface, a large zone void of 'attaching' proteins forms (*i.e.* depletion zone), in time, from the surface of the crystal extending outwards into the solution. With the formation of the depletion zone, the local concentration adjacent to the crystal can be far different from the bulk solution. Hence, the rate of crystal growth becomes slowed and non-linear behavior subsequently arises. Formally, the solute flux towards the crystal face, j_{in}, is expressed in terms of the solute diffusion coefficient, D, and a concentration gradient, ∇c, as

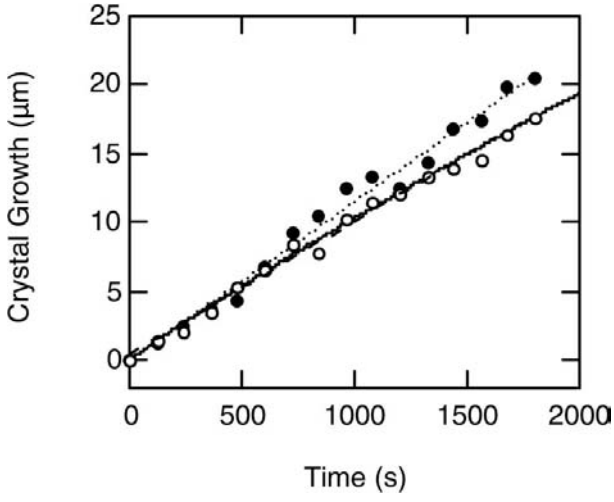

Figure 1
Growth of (110) face of tetragonal lysozyme crystal, in time, in solution conditions of 0.1 *M* NaAc pH 5.0 with 4% NaCl at a temperature of 296 K is shown. The empty and filled circles represent data obtained from two different crystals. The solid line represents a numerical solution of (6) (see text) that best exemplifies the measured data. The dashed line is a linear fit to the data.

$$j_{in} = D\nabla c \simeq D\Delta c/w, \tag{4}$$

where Δc represents the difference between the protein concentration in solution and the crystal/solution interface over a distance w, and $w \simeq (Dt)^{1/2}$ is the mean diffusion width of the 'depletion zone' that varies as the square root of time t. The balancing crystal flux, j_{crys}, in terms of a crystal-growth velocity, V_x and the protein concentration within the crystal, c_x, for the limited case of high growth velocities, is expressed as

$$j_{crys} = V_x c_x,\ V_x = \beta(c_i - c_{eq}), \tag{5}$$

where β is a kinetic coefficient of macromolecular attachment to a crystal surface, c_i is the solute concentration at the crystal/solution interface and c_{eq} is the equilibrium solute concentration at which the crystal ceases to grow. Under conditions of rapid growth and $c_\infty, c_i >> c_{eq}$, the solute concentration at the crystal interface, in time, is approximated by

$$c_i = \frac{c_\infty}{1 + \beta c_x (t/D)^{1/2}}. \tag{6}$$

As (6) is recursive, numerical methods were applied to provide a quantitative means for the dependence of c_i in terms of the initial solute concentration, c_∞, diffusion coefficient, D, and the crystal concentration, c_x. The solid line in Fig. 1 represents a numerical solution of (6) using the initial parameters $D \simeq 1 \times 10^{-6}$ cm^2 s^{-1}, $V_x \simeq 1.3 \times 10^{-6}$ cm s^{-1}, $c_x \simeq 800$ mg ml^{-1} and $c_\infty \simeq 60$ mg ml^{-1}. Over the period that the crystal growth was measured, crystal-growth velocity varied from $V_x \simeq 1.27$ to 0.97×10^{-6} cm s^{-1} or an average value of $1.1 \simeq 10^{-6}$ cm s^{-1}, which was also reasonably estimated by a linear fit to the data.

In addition to the determination of growth velocities, (6) also provides estimates for the maximum amount of time for crystal-growth observations before non-linear behavior is expected. For example, non-linear behavior can be expected to occur when the interfacial concentration is reduced to one-half the initial solute concentration. $c_i \simeq c_\infty/2$ when the time varying component in the denominator approaches unity. The maximum observation period for crystal growth is

$$t = \frac{D}{V_x^2}\left(\frac{c_\infty}{c_x}\right)^2. \tag{7}$$

For conditions illustrated in Fig. 1, with $D \simeq 1 \times 10^{-6}$ cm^2 s^{-1}, $V_x \simeq 1.3 \times 10^{-6}$ cm s^{-1}, $c_x \simeq 800$ mg ml^{-1} and $c_\infty \simeq 60$ mg ml^{-1}, the time required to induce a factor of 2 change in the crystal growth rate is ~5600 s. Crystal-growth observations for periods much shorter than the maximum defined by (7) are then considered to not contribute significantly to errors in the determination of crystal-growth velocities. Moreover, (7) provides a qualitative understanding of the observation that solutions of low protein concentration often give rapid rise to non-linear behavior in crystal growth at high growth velocities.

The overall significance of (7) is that it provides reasonable estimates for the maximum measurement period, independent of the method applied. It should be noted, however, that (6) and (7) represent the limiting case where solution convection is negligible. The presence of convention would render the assumption $w \simeq (Dt)^{1/2}$ invalid, as it may assume a fixed length that is time invariant. Under convective conditions, the measurement periods can far exceed predictions provided by (6) and (7). Nevertheless, further examinations of interface concentration, c_i, for a variety of conditions would be required to assess the validity of (6) and (7), a subject for future discussion.

3. Determination of a kinetic crossover from growth velocity measurements

The dependence of crystal growth velocities with respect to temperature offers the simplest means for determining the possible existence of a kinetic crossover. For example, Fig. 2 is an Arrhenius plot of the natural logarithm of the (110) face growth velocities as a function of inverse temperatures. The growth-velocity measurements were performed using an optical microscopic method following established protocols (Pusey, 1993). Moreover, the growth-velocity measurements were obtained for the solution conditions of 0.05 *M* NaAc maintained at pH 4.5 with 2.5% NaCl, as the solution temperature, T, was varied.

As shown in Fig. 2, the Arrhenius diagram readily identifies two separate regions attributable to either different crystal growth processes or phase transitions. That is, a deviation from the expected linear behavior in the growth velocity data is observed at a temperature designated as T_{dev}. As the liquid–liquid phase transition does not contribute to the occurrence of the observed deviation in growth velocity data (Gorti, Konnert *et al.*, 2005), T_{dev} simply represents the deviation point in the measured growth velocity that most likely occurs as a result of a change in the growth mechanism. At $T < T_{dev}$, growth-velocity data were interpreted using a parametric relation for the unknown quantities of the natural logarithm of (1), whereas at temperatures $T > T_{dev}$, growth-velocity data were interpreted using a parametric relation for the unknown quantities of the natural logarithms of (2). In Fig. 2, the dotted and solid lines are computer-generated fit to the natural logarithm of (1) and (2), respectively, that best characterize crystal-growth velocities within the respective limits of the applicability of the models. The estimated effective step free energy is $\gamma = 1.2 \times 10^{-13}$ erg/molecule, the energy barrier associated with continuous growth is $E_c = 8 \times 10^{-13}$ erg/molecule and the average crossover concentration is $c_r \simeq 6.5 \times c_{eq}$ or $\sigma_c = 1.9$.

It should be noted that estimates for γ, E_c and σ_χ can be obtained from the analyses of growth-velocity data only if accurate measurements of the solubility, $c_{eq}(T)$, over the experimental range of temperatures are also available. In the present case, the magnitude of $c_{eq}(T)$ was extrapolated from previously published values (Cacioppo & Pusey, 1991; Forsythe, Judge *et al.*, 1999). Although the extrapolated values for c_{eq} are not considered to contribute significantly to the error in the estimation of γ, E_c and σ_c, the magnitudes of the values presented should, nevertheless, be interpreted with caution. Regardless of the present ambiguities, growth velocity data indeed indicate a change in the growth mechanism readily identifiable as a deviation in the expected linear behavior in an Arrhenius plot.

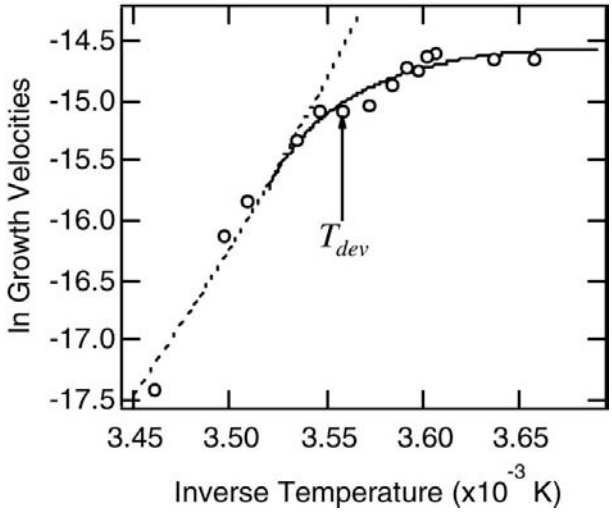

Figure 2
The dependence of the (110) face growth velocities of tetragonal lysozyme on temperature. The dashed line is a computer-generated fit to the natural logarithm of (1) that best characterizes crystal growth by two-dimensional nucleation. The solid line is obtained using the natural logarithm of (2) that best represents crystal growth by the continuous mode.

4. Application of atomic force microscopy in crystal growth

Initial applications of atomic force microscopy (AFM) were limited to the characterization of the surface properties of lysozyme crystals (Durbin & Carlson, 1992; Konnert *et al.*, 1994). Subsequent groups have investigated many features of crystal growth that occur on a time scale amenable to direct visualization. However, AFM applications have been predominantly limited to investigations of crystal growth mechanisms, defect formations, impurity incorporation *etc.* and have been reviewed elsewhere (McPherson *et al.*, 2000, 2001). In addition, AFM has been applied not only to investigate directly the growth kinetics and associated thermodynamics (Malkin *et al.*, 1995; Rong *et al.*, 2000; Yau *et al.*, 2000), but also to determine explicitly the molecular 'packing' on crystal surfaces (Konnert *et al.*, 1994; Li *et al.*, 1999).

AFM is regarded as a powerful tool for providing details of the crystal growth processes at the molecular level. For example, available physical models describing crystal growth (*i.e.* equations 1 and 2) cannot *a priori* predict the mode by which a crystal grows. That is, the mode of crystal growth cannot be determined solely on the basis of experimental measurements of the magnitude of either the concentration/supersaturation or crystal-growth velocity. Hence, the application of any theoretical model describing growth velocity within a given range of concentration or supersaturation should be experimentally justified, preferably by an independent means. Observation of crystal growth using AFM can readily provide visual details of the crystal-growth processes at the molecular level, thereby establishing the limits of applicability of the various models for crystal-growth velocity measurements. In addition, visual estimations of the size of a critical nucleus have also been applied to determine the energetics of crystal growth (Malkin *et al.*, 1995; Rong *et al.*, 2000; Yau *et al.*, 2000).

In the present effort, AFM is applied to determine the energetics as well as possibly the kinetic roughening transition of lysozyme crystal growth. In particular, analyses of spatial fluctuations (noise) in the height, $h(x)$, on the surface of a growing crystal using methods established in fluctuation spectroscopy are presented (Kittel, 1958; Weissman, 1976). It should be noted, however, that the estimation of the energetics of crystal growth as given below precedes any adequate theory and should be applied with caution. Methods for analyses of roughness exponents from $h(x)$ in the estimation of a kinetic roughening are, however, well established (Kardar *et al.*, 1986; Tartaglino & Levi, 2000; Das Sarma *et al.*, 2002).

The schematic diagram (Fig. 3) exhibits a stationary view of the crystal-growth process leading eventually to a kinetic roughening transition. From the outset, it is assumed that a lateral correlation length on the surface, ξ, exists, as the surface grows layer by layer. The magnitude of the correlation length is assumed to be independent of time (*i.e.* stationary) at a fixed supersaturation and can be determined by the autocorrelation function of the spatial fluctuations in height of the surface, $h(x)$. Moreover, the root-mean-square (r.m.s.) magnitude of fluctuations $(\langle h^2\rangle - \langle h\rangle^2)^{1/2}$ is also considered to be invariant, in time, for a given supersaturation as the surface grows by two-dimensional nucleation. The behavior of the magnitudes of both ξ

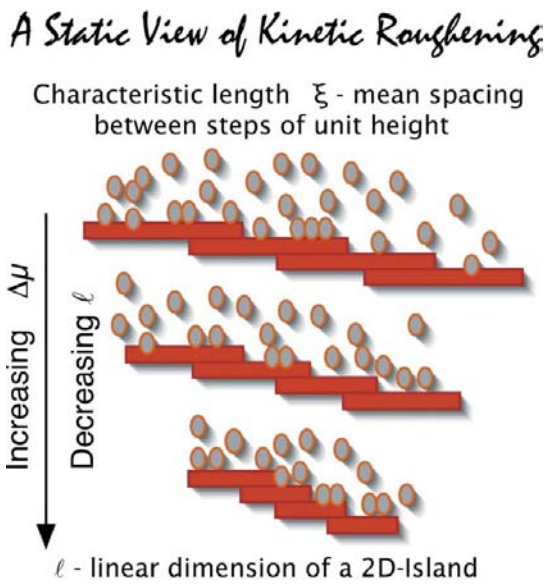

Figure 3
Representation of processes leading up to a kinetic roughening transition.

and $(\langle h^2\rangle - \langle h\rangle^2)^{1/2}$ on the surface of a 'smooth' crystal are expected to be divergent, as the solution saturation is increased (Tartaglino & Levi, 2000). Namely, ξ decreases while $(\langle h^2\rangle - \langle h\rangle^2)^{1/2}$ increases as the solution supersaturation is increased up to the crossover supersaturation, σ_c. The decrease in ξ is, in part, predictable as the size of the two-dimensional island, ℓ, is expected to decrease along with the number of particles, $N^*_{2\mathrm{Dnuc}}$, within a critical nucleus according to (3). The lowering of $\Delta G^*_{2\mathrm{Dnuc}}$ with respect to increasing supersaturation, also according to (3), increases the magnitude of $(\langle h^2\rangle - \langle h\rangle^2)^{1/2}$ due to the expected increase in the nucleation rate, J. Beyond σ_c, however, $h(x)$ cannot be assumed to be stationary and interpretation of the height profile becomes modified, in time (Kardar *et al.*, 1986; Tartaglino & Levi, 2000; Das Sarma *et al.*, 2002; Zhao *et al.*, 2000).

Fig. 4 exhibits an AFM image of the surface of the (101) face of a tetragonal lysozyme crystal under conditions of growth by two-dimensional nucleation, as well as a height profile $[h(x) - \langle h(x)\rangle]$ at a fixed y-position. AFM images were obtained as follows. (i) Lysozyme crystals in solution conditions of 0.1 *M* NaAc pH 5.0 and 4% NaCl were prepared using a batch method in sitting-drop wells. (ii) A tetragonal crystal was selected with an optical microscope for the AFM measurement. (iii) Upon removal from the well, the crystal was immediately placed in a 50 µl drop of protein solution, containing 5 mg ml^{-1} in 0.1 *M* NaAc pH 5.0 with 4% NaCl, resting on a cover glass. (iv) The cover glass was then affixed to a Teflon well and an additional 150 µl of protein solution was added to the well. Finally, the crystal within the cover glass/Teflon well was finally placed on the temperature-controlled stage and brought into contact with a cantilever for imaging by AFM. The AFM system used in this experiment is a commercially available instrument, Picoscan, purchased from Molecular Imaging. The x–y range of the scanner was $\sim$7 × 7 µm. Commercially available cantilevers with a spring constant of 0.05 N m^{-1}, resonance frequency $\sim$25 KHz and Si_3N_4 tips were used to image the crystal surfaces.

The temperature of the AFM experiments was initially maintained at 293 K and subsequently varied to obtain images at higher supersaturations using solutions of fixed protein concentration. In all cases, crystals were replaced between each supersaturation investigated to ensure a 'smooth' crystal face as an initial condition, prior to modifying the solution supersaturation. At given supersaturation, two

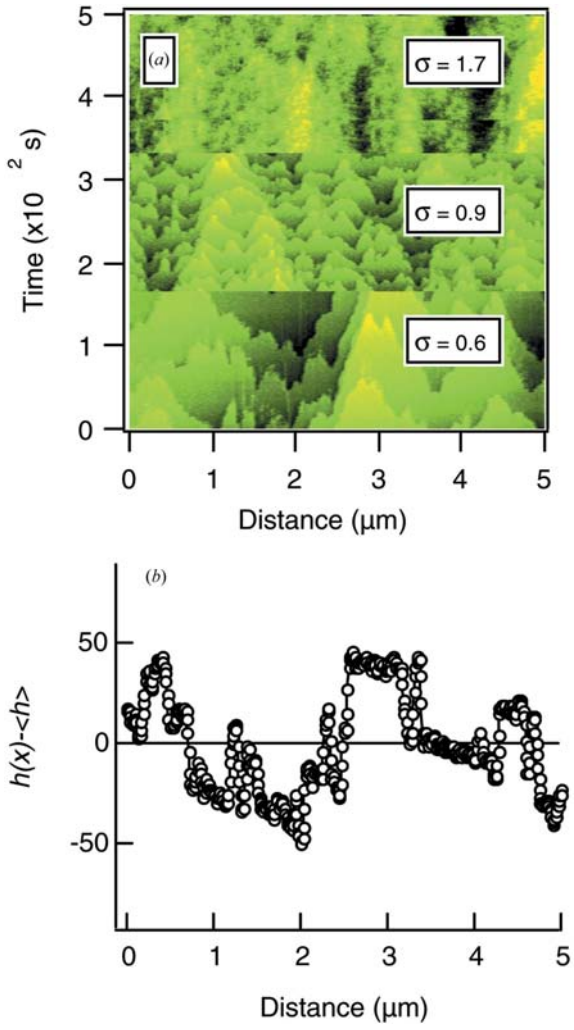

Figure 4
Image of the (101) face of tetragonal lysozyme under conditions of growth is exhibited. The AFM image, in (*a*), is a composite of 'line scan' images obtained at various σ. In (*b*), the height profile as a function of position is exhibited.

distinct modes of data collection were performed: imaging of a 5 × 5 µm^2 area or a line scan of 5 µm in length (see Fig. 4a). Although both modes of data collection yielded essentially the same results (see below), measurements performed in the line-scan mode enabled data collection at significantly higher supersaturations. Regardless of the mode of data collections, all AFM measurements were obtained using an intermittent contact mode.

From AFM images, fluctuations in $h(x)$ (see Fig. 4*b*) which represent changes in unit height at every step-edge at a given position, x are obtained. For the stationary case $t = 0$ for each y position scanned, the autocorrelation function of the fluctuations in $h(x)$ is

$$C(x) = \langle h(0)h(x)\rangle = \sum_i A_i \exp(-\xi_i x), \tag{8}$$

with

$$\langle h^2\rangle = \sum_i A_i$$

and

$$\langle h\rangle^2 = \lim_{x\to\infty} \sum_i A_i \exp(-\xi_i x)$$

where the angle brackets denote an ensemble average of a stationary process giving rise to a random spatial variation in $h(x)$. The evaluation of the highly non-exponential spatial autocorrelation functions (see Fig. 5) was performed using a single exponential method for a limited range of the calculated correlation functions. Fig. 5(*a*) exhibits spatial autocorrelation functions calculated from AFM images obtained at five different supersaturations. Although the data in Fig. 5(*a*) exhibit non-exponential behavior, the remarkable feature of the data is the rapid decrease of the correlation functions as the supersaturation is increased. In Fig. 5(*b*), the 'equal time' height–height correlation functions $H(x) = \{[h(x)-h(0)]^2\} = 1 - C(x)/\langle h^2\rangle$ are displayed (Zhao *et al.*, 2000). Under the conditions $x << \xi$, $H(x) \simeq x^{2\alpha}$, where α is a roughness exponent (Das Sarma *et al.*, 2002). The magnitude of α ranged from 0.6 to 1.0 as the solution supersaturation approached, possibly indicating a kinetic roughening transition (Das Sarma *et al.*, 2002).

Fig. 6 displays the behavior of the average correlation length ξ, as well as the magnitude of the r.m.s. amplitude of $h(x)$ as a function of supersaturation that were obtained upon analyses of the calculated spatial correlation functions, according to (8). The remarkable features of the data are the rapid decrease and asymptotic behavior in the average correlation length ξ as the supersaturation is increased. To the contrary, the r.m.s. amplitude of fluctuations in $h(x)$, $(\langle h^2\rangle - \langle h\rangle^2)^{1/2}$, increased gradually as the supersaturation increased. The observed divergent behavior in ξ and $(\langle h^2\rangle - \langle h\rangle^2)^{1/2}$ is directly related to their dependence on the two-dimensional island formation or nucleation rate J, where $\xi \simeq naJ$ and $(\langle h^2\rangle - \langle h\rangle^2)^{1/2} \simeq naJ^{-1}$. The nucleation rate, J, is given as (Saito, 1996):

$$J \simeq B\sigma^{1/2} \exp(-\pi\gamma^2/k_B T\Delta\mu), \quad (9)$$

where B is a constant. The solid and dashed lines in Fig. 6 are computer-generated fit to data for J^{-1} and J, respectively, using $\gamma \simeq 1.8 \times 10^{-4}$ erg/molecule for both cases. Although γ from determinations of ξ and $(\langle h^2\rangle - \langle h\rangle^2)^{1/2}$ is nearly one order of magnitude less than γ estimated from microscopic growth-velocity measurements, both values become comparable when γ estimated from optical microscopic measurements is normalized by N^*_{2Dnuc}.

At present, we are unaware of any theoretical models that predict the observed differences in the estimation of γ from either microscopic or molecular-level measurements. Taking into consideration the number of approximations applied in the determination of γ from molecular-level measurements, any suggested difference might well be due to experimental artifacts, *i.e.*, the formation of a depletion zone according to (6) and (7). More significant than the estimation of γ is the asymptotic behavior of ξ. Namely, the data indicate a general independence of ξ with respect to growth velocity at higher supersaturations: a condition predictive of kinetic roughening (Das Sarma *et al.*, 2002). Moreover, the data exhibited in Fig. 6 do not exhibit critically divergent behavior between ξ and $(\langle h^2\rangle - \langle h\rangle^2)^{1/2}$. As critical divergence is neither observed nor expected to occur, the preliminary data do not support the hypothesis of a first-order transition (Tartaglino & Levi, 2000). Predictably, the crossover behavior appears to be continuous and thus may not represent a first-order transition (Hwa *et al.*, 1991). As the current study is preliminary, further work is required to detail the behavior of the various parameters that are predictive of a kinetic roughen transition. Regardless, the methods established may be applied to detail the phenomena of kinetic roughening and possibly thermodynamic roughening of protein crystals: a subject for future investigation.

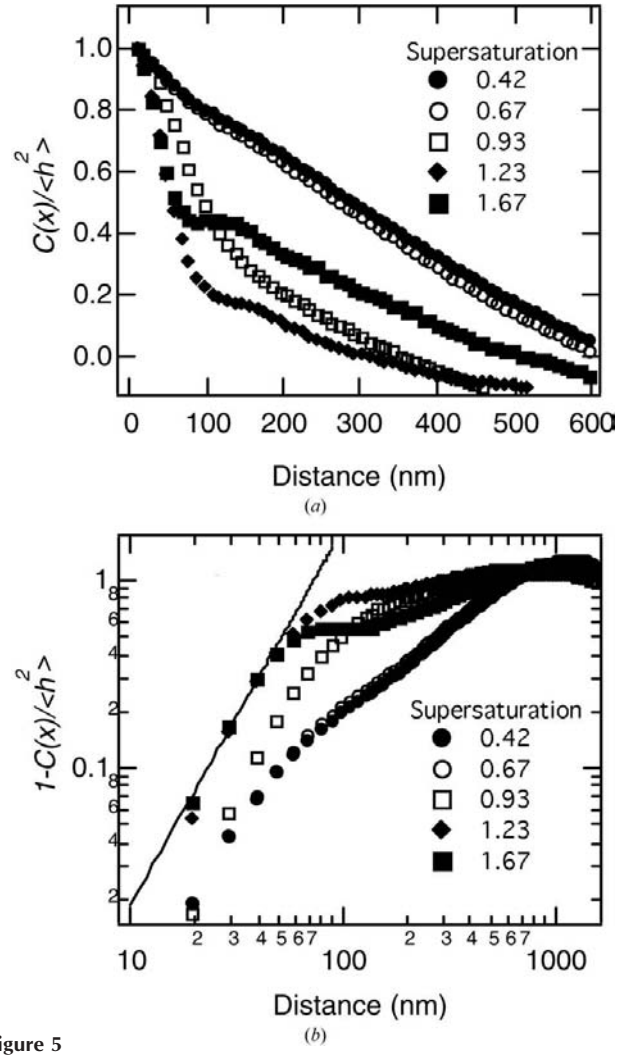

Figure 5
In (*a*), the spatial autocorrelation functions calculated from AFM images obtained at five different supersaturations are presented. In (*b*), the height–height correlation functions $H(x)$ of data in (*a*) are displayed. The solid line in (*b*) represents $x^{2\alpha}$, where x is the distance and α is a roughness exponent set equal to 1.0 (see text).

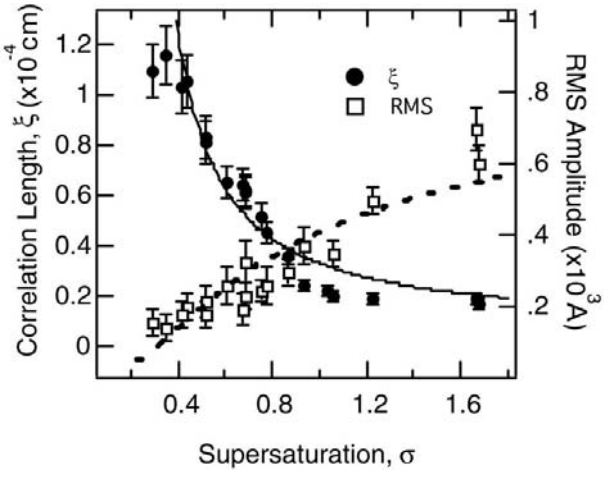

Figure 6
The dependence of ξ (solid circles) and $(\langle h^2\rangle - \langle h\rangle^2)^{1/2}$ (open squares) as a function of solution supersaturation. The solid and dashed lines are computer generated fit to data using a parametric relation for (9).

References

Bennema, P. (1993). *J. Phys. D*, **26**, B1–B6.
Cacioppo, E. & Pusey, M. L. (1991). *J. Cryst. Growth*, **114**, 286–292.
Das Sarma, S., Punyindu Chatraaphorn, P. & Toroczkai, Z.(2002). *Phys. Rev. E.* **65**, 036144.
Durbin, S. & Carlson, W. E. (1992). *J. Cryst. Growth*, **122**, 71–79.
Durbin, S. & Feher, G. (1986). *J. Cryst. Growth*, **76**, 583–592.
Elwenspoek, M. & van der Eerden, J. P. (1987). *J. Phys. A*, **20**, 669–678.
Forsythe, E. L., Ewing, F. L. & Pusey, M. L. (1994). *Acta Cryst.* D**50**, 614–619.
Forsythe, E. L., Judge, R. A. & Pusey, M. L. (1999). *J. Chem. Eng. Data*, **44**, 637–640.
Forsythe, E. L., Nadarajah, A. & Pusey, M. L. (1999). *Acta Cryst.* D**55**, 1005–1011.
Forsythe, E. L. & Pusey, M. L. (1994). *J. Cryst. Growth*, **139**, 89–94.
Gorti, S., Forsythe, E. L. & Pusey, M. L. (2004). *Cryst. Growth Des.* **4**, 691–699.
Gorti, S., Forsythe, E. L. & Pusey, M. L. (2005). *Cryst. Growth Des.* **5**, 473–482.
Gorti, S., Konnert, J., Forsythe, E. L. & Pusey, M. L. (2005). *Cryst. Growth Des.* **5**, 535–545.
Hwa, T., Kardar, M. & Paczuski, M. (1991). *Phys. Rev. Lett.* **66**, 441–444.
Kardar, M., Parisi, G. & Zhang, Y.-C. (1986). *Phys. Rev. Lett.* **56**, 889–892.
Kittel, C. (1958). *Elementary Statistical Physics.* New York: Wiley.
Konnert, J. H., D'Antonio, P. & Ward, K. B. (1994). *Acta Cryst.* D**50**, 603–613.
Kurihara, K., Miyashita, S., Sazaki, G., Nakada, T., Suzuki, Y. & Komatsu, H. (1996). *J. Cryst. Growth*, **166**, 904–908.
Kuznetsov, Y. G., Malkin, A. J., Glantz, W. & McPherson, A. (1996). *J. Cryst. Growth*, **168**, 63–73.
Levi, A. C. & Kotrla, M. (1997) *J. Phys. Condens. Matter*, **9**, 299–344.
Li, H., Perozzo, M. A., Konnert, J. H., Nadarajah, A. & Pusey, M. L. (1999). *Acta Cryst.* D**55**, 1023–1035.
Liu, X.-Y. & Bennema, P. (2001) *J. Chem. Phys.* **115**, 4268–4274.
Liu, X.-Y., van Hoof, P. & Bennema, P. (1993). *Phys. Rev. Lett.* **71**, 109–112.
Malkin, A. J., Kuznetsov, Y. G., Land, T. A., McPherson, A. & DeYoreo, J. J. (1995). *Phys. Rev. Lett.* **75**, 2778.
McPherson, A., Malkin, A. J. & Kuznetsov, Y. G. (2000). *Annu. Rev. Biophys. Biomol. Struct.* **29**, 361–410.
McPherson, A., Malkin, A. J., Kuznetsov, Y. G. & Plomp, M. (2001). *Acta Cryst.* D**57**, 1053–1060.
Monaco, L. A. & Rosenberger, F. (1993). *J. Cryst. Growth*, **129**, 465–484.
Nadarajah, A., Forsythe, E. L. & Pusey, M. L. (1995). *J. Cryst. Growth*, **151**, 163–172.
Pusey, M. L. (1993). *Rev. Sci. Instrum.* **64**, 3121–3125.
Pusey, M. L., Snyder, R. S. & Nauman, R. (1986). *J. Biol. Chem.* **261**, 6524–6529.
Rong, L., Yamane, T. & Niimura, N. (2000). *J. Cryst. Growth*, **217**, 161–169.
Saito, Y. (1996). *Statistical Physics of Crystal Growth.* Singapore: World Scientific.
Tartaglino, U & Levi, A. C. (2000). *Physica A*, **277**, 83–105.
Vekilov, P. G. (1993). *Prog. Cryst. Growth*, **26**, 25–49.
Weissman, M. B. (1976). PhD Dissertation, Department of Physics, University of California, San Diego, USA.
Yau, S. T., Petsev, D. N., Thomas, B. R. & Vekilov, P. G. (2000). *J. Mol. Biol.* **303**, 667–678.
Zhao, Y.-P., Fortin, J. B., Bonvallet, G., Wang, G.-C. & Lu, T.-M. (2000). *Phys. Rev. Lett.* **85**, 3229–3232.